Journal of Experimental Botany, Vol. 73, No. 1 pp. 275–291, 2022
https://doi.org/10.1093/jxb/erab435 Advance Access Publication 23 September 2021

RESEARCH PAPER

Dissecting the metabolic reprogramming of maize root under nitrogen-deficient stress conditions

Niaz Bahar Chowdhury[1], Wheaton L. Schroeder[1], Debolina Sarkar[2], Nardjis Amiour[3], Isabelle Quilleré[3], Bertrand Hirel[3], Costas D. Maranas[2] and Rajib Saha[1,4,*]

[1] Department of Chemical and Biomolecular Engineering, University of Nebraska-Lincoln, Lincoln, NE, USA
[2] Department of Chemical Engineering, The Pennsylvania State University, University Park, PA, USA
[3] Institut National de Recherche pour l'Agriculure, l'Alimentation et l'Envionnement (INRAE), Centre de Versailles-Grignon, RD 10, 78026 Versailles cedex, France
[4] Center for Root and Rhizobiome Innovation, University of Nebraska-Lincoln, Lincoln, NE, USA

* Correspondence: rsaha2@unl.edu

Received 10 May 2021; Editorial decision 14 September 2021; Accepted 21 September 2021

Editor: Yves Gibon, INRAE, France

Abstract

The growth and development of maize (*Zea mays* L.) largely depends on its nutrient uptake through the root. Hence, studying its growth, response, and associated metabolic reprogramming to stress conditions is becoming an important research direction. A genome-scale metabolic model (GSM) for the maize root was developed to study its metabolic reprogramming under nitrogen stress conditions. The model was reconstructed based on the available information from KEGG, UniProt, and MaizeCyc. Transcriptomics data derived from the roots of hydroponically grown maize plants were used to incorporate regulatory constraints in the model and simulate nitrogen-non-limiting (N^+) and nitrogen-deficient (N^-) condition. Model-predicted flux-sum variability analysis achieved 70% accuracy compared with the experimental change of metabolite levels. In addition to predicting important metabolic reprogramming in central carbon, fatty acid, amino acid, and other secondary metabolism, maize root GSM predicted several metabolites (l-methionine, l-asparagine, l-lysine, cholesterol, and l-pipecolate) playing a regulatory role in the root biomass growth. Furthermore, this study revealed eight phosphatidylcholine and phosphatidylglycerol metabolites which, even though not coupled with biomass production, played a key role in the increased biomass production under N-deficient conditions. Overall, the omics-integrated GSM provides a promising tool to facilitate stress condition analysis for maize root and engineer better stress-tolerant maize genotypes.

Keywords: Abiotic stress, genome-scale metabolic modeling, maize root, metabolomics, nitrogen-deficient stress, transcriptomics.

Abbreviations: C, carbon; CCM, central carbon metabolism; DIMBOA, 2,4-dihydroxy-7-methoxy-1,4-benzoxazin-3-one; FBA, flux balance analysis; FSA, flux-sum analysis; FVA, flux variability analysis; GPR, gene–protein reaction; GSM, genome-scale metabolic model; MAX2, more axillary growth 2; N, nitrogen; N^+, nitrogen-non-limiting; N^-, nitrogen-deficient; PC, phosphatidylcholine; PG, phosphatidylglycerol; PP, pentose phosphate; TCA, tricarboxylic acid; WT, wild type.

Introduction

Maize (*Zea mays* L.) is considered as one of the major sources of food for a large portion of the world's population (Rouf Shah *et al.*, 2016). According to the International Grains Council, global maize consumption will climb to new heights in the coming years, and the use of maize as food is also forecast to expand (International Grains Council, 2019). Nutrients that are taken up by roots are essential for maize plant growth, and limited nutrient supply can hinder plant growth along with discernible phenotypical changes (Hu and Chu, 2020). Among these nutrients, nitrogen (N) plays a key role in plant growth. N limitation frequently reduces crop growth and yield, and contributes to a variety of phenotypical changes including expanded root architecture (Mager and Ludewig, 2018), increased root biomass (Mardanov *et al.*, 1998), and root exudate profiles (Frey *et al.*, 2009; Neal *et al.*, 2012). Although many experimental studies are available that study the metabolism associated with N starvation of maize roots (Tschoep *et al.*, 2009; Krapp *et al.*, 2011; Schlüter *et al.*, 2012; Mager and Ludewig, 2018), they are primarily focused on probing a specific class of metabolites, such as amino acids or fatty acids. However, capturing the aggregate effect of maize root physiology on biomass production under N-deficient (N^-) condition is essential to understand plant-wide reprogramming of its metabolism. This sort of reprogramming has been reported as the hallmark of metabolism which allows any system to adapt to the changes to external conditions (Medina, 2020). Thus, in order to capture this metabolic reprogramming of maize root under N^- condition in an integrated manner, developing systems biology approaches will allow us to have a dynamic picture of plant adaptation to N deficiency.

To develop such a systems biology approach, genome-scale metabolic models (GSMs) have been widely used at either the organ or the whole-plant level (Shaw and Cheung, 2020). A GSM captures most of the known metabolic reactions within a biological system (i.e. a prokaryotic/eukaryotic organism or an organ/group of organs of a higher order organism) and it can predict the flux of reactions by implementing techniques such as flux balance analysis (FBA) (Orth *et al.*, 2010), flux variability analysis (FVA) (Mahadevan and Schilling, 2003), and parsimonious FBA (Lewis *et al.*, 2010). Typically, reaction flux is predicted by solving an optimization problem through maximizing biomass production. In higher plants, the first GSM was reconstructed for *Arabidopsis thaliana* more than a decade ago (Poolman *et al.*, 2009), thus setting up a new direction of research with the aid of systems biology. Once the complete genome sequences of more plants became available, metabolic reconstruction picked up pace, giving a range of published plant GSMs, including crops such as maize (Saha *et al.*, 2011), rice (*Oryza sativa* L.) (Poolman *et al.*, 2013; Chatterjee *et al.*, 2017), and rapeseed (*Brassica napus* L.) (Pilalis *et al.*, 2011), and model plants such as Arabidopsis (Poolman *et al.*, 2009; de Oliveira Dal'Molin *et al.*, 2010; Cheung *et al.*, 2013) and *Setaria viridis* L. (Shaw and Cheung, 2019). Although these GSMs provided reconstruction of whole-plant metabolism, organ-specific GSMs including those of rapeseed embryo (Hay and Schwender, 2011), barley seed (Grafahrend-Belau *et al.*, 2009), Arabidopsis leaf (Arnold and Nikoloski, 2014), and maize leaf (Simons *et al.*, 2014; Seaver *et al.*, 2015), endosperm (Seaver *et al.*, 2015), and embryo (Seaver *et al.*, 2015) were developed in parallel. These organ-specific GSMs provided better resolution of the metabolism in specialized tissues, which can be probed further for useful insights into whole-plant physiology. Up to now, there has been no maize root-specific GSM available to investigate its metabolism/associated reprogramming under stress conditions, such as mineral nutrient deficiency, and derive new biological insights that can be tested experimentally.

An important challenge to further sharpen model predictions and thereby decipher meaningful biological information from a GSM is to integrate environment/condition-specific 'omics' data into it. Although there is a paucity of environment-specific 'omics' data (i.e. gene expression, protein abundance, and metabolite level) for maize root, their availability would help constrain the solution space and thus improve final model predictions. Proteomics and transcriptomics data can be used to apply flux constraints on corresponding reactions determined by gene–protein reaction (GPR) associations via a switch [e.g. GIMME (Becker and Palsson, 2008), iMAT (Zur *et al.*, 2010), and MADE (Jensen and Papin, 2011)] or valve [e.g. E-Flux (Colijn *et al.*, 2009) and PROM (Chandrasekaran and Price, 2010)] approach. While the switch approaches have a binary nature, resulting in all-or-nothing posture to constraining reactions which may not reflect the actual condition, valve approaches provide more flexibility in constraining the solution space by incorporating the gene expression/protein abundance data as reaction flux constraints. In addition to incorporating these reaction regulations, model-generated metabolite levels can be qualitatively compared with experimental metabolite measurements, thus further characterizing the state of metabolism. To this end, flux-sum is used as a proxy of the metabolite pool size (Chung and Lee, 2009). However, fast or slow kinetics may diminish or expand the size of the pool, without changing the corresponding flux.

In this work, maize plants were grown in a hydroponic culture system under nitrogen-non-limiting (N^+) and N^- condition, and used to generate root transcriptomics and metabolomics datasets. In parallel, a GSM was built for roots in order to incorporate transcriptomic and metabolic profiling data into the model to simulate the metabolic reprogramming of maize roots under N^- condition. The model was first validated using a study from the literature (Walton *et al.*, 2016) on the effect of the synthetic strigolactone, rac-GR24, on the root and its associated metabolic reprogramming. Next, using the E-Flux algorithm (Colijn *et al.*, 2009), the transcriptomics data were employed to implement regulations in the GSM and subsequently to simulate N^+ and N^- condition. When compared with metabolite measurements, the model-predicted results achieved 70% accuracy

concerning the reprogramming of central carbon (C), fatty acid, amino acid, and secondary metabolism. In addition, the GSM allowed the prediction of regulatory roles of several metabolites in root biomass production, such as L-methionine, L-asparagine, L-lysine, cholesterol, and L-pipecolate. Eight phosphatidylcholine (PC) and phosphatidylglycerol (PG) metabolites not coupled to biomass production under N^+ conditions were found to play a seminal role in the increased biomass growth under N^-. Going forward, we expect that this maize root GSM will provide a powerful tool to study the effect of other abiotic and biotic stresses such as phosphate deficiency, salinity, heat stress, drought, heavy metal stresses, rot disease, and interactions with beneficial microorganisms.

Materials and methods

Plant material

Zea mays L., line B73 (Hufford *et al.*, 2021), were grown in a hydroponic culture system. To eliminate heterogeneity in the germination time, imbibition of the seeds was performed at 6 °C in the dark for 3 d in Petri dishes containing filter paper moistened with sterile distilled water. Seedlings were then transferred onto sand and watered daily on a nutrient solution containing 5.6 mM K^+, 3.4 mM Ca^{2+}, 0.9 mM Mg^{2+}, 0.9 mM $H_2PO_4^-$, and 21.5 mM Fe (Sequestrene, Ciba-Geigy, Basel), 23 mM B, 9 mM Mn, 0.30 mM Mo, 0.95 mM Cu, and 3.50 mM Zn. N was supplied as 1 mM KNO_3^-. After 1 week when 2–3 leaves had emerged, plants were randomly placed on a 130 liter aerated hydroponic culture unit containing a complete nutrient solution (N^+) containing 5 mM NO_3^- (Coïc and Lesaint, 1971) together withi 5 mM K^+, 3 mM Ca^{2+}, 0.4 mM Mg^{2+}, 1.1 mM $H_2PO_4^-$, 1 mM SO_4^{2-}, 1.1 mM Cl^-, 21.5 μM Fe^{2+} (Sequestrene), 23 μM B^{3+}, 9 μM Mn^{2+}, 0.3 μM Mo^{2+}, 0.95 μM Cu^{2+}, and 3.5 μM Zn^{2+}. For growing plants under N^- condition, NO_3^- was supplied as 0.1 mM KNO_3^-, an N concentration that has previously been shown to provide N deficiency stress for most plant species (Tercé-Laforgue *et al.*, 2004; Hirel *et al.*, 2005; Amiour *et al.*, 2012). The N^+ and N^- nutrient solutions were replaced daily. The experiment was performed in triplicate for each N concentration in the nutrient solution in separate hydroponic units placed side by side. The six hydroponic culture units were kept for 18 d in a controlled-environment chamber in 2014 (18 May–5 June 2014). Three plants in each hydroponic unit were pooled, making three replicates for each of the two conditions. Plants were harvested at the 6- to 7-leaf stage between 09.00 h and 12.00 h, and separated into shoots and roots. The samples were immediately placed in liquid N_2 and then stored at –80 °C until further analysis.

RNA preparation

A 50 mg aliquot of total RNA was incubated at 37 °C for 30 min with 40 U of RNase inhibitor and 25 U of RNase-free DNase (Promega, Charbonnieres, France) in 6 ml of 10× buffer (Promega) with diethylpyrocarbonate (DEPC)-treated water added to a final volume of 60 ml. The DNase was removed by phenol/chloroform/isoamyl alcohol (25:24:1) extraction, and total RNA was precipitated overnight at –20 °C in a 0.1 vol. of ammonium acetate (3 M) and a 2.5 vol. of ethanol (100%), and resuspended in DEPC-treated water.

Gene expression profiles using maize cDNA microarrays

Starting with 3 μg of root total RNA, non-modified amplified antisense RNA (aRNA) products were prepared using the Amino Allyl MessageAmp™ aRNA Kit (Ambion, Foster City, CA, USA), according to the manufacturer's instructions. Briefly, RNA was transcribed into cDNA using reverse transcriptase with a T7 primer that contains a promoter for DNA-dependent RNA polymerase. After RNase H-mediated second-strand cDNA synthesis, the double-stranded cDNA (dscDNA) was purified and served as a template in the subsequent *in vitro* transcription reaction. Following this, 2 μg aliquots of aRNA were labeled using the SuperSript™ Indirect cDNA Labeling System Kit (Invitrogen, Carlsbad, CA, USA) as described in the manufacturer's protocol, except that the purification steps were carried out using QIAquick® PCR columns (QIAGEN, Hilden, Germany). The quantity and quality of each intermediate product, including total RNA, dscDNA, aRNA, and labeled targets, were evaluated using a Nanodrop ND-1000 spectrophotometer and an Agilent Technologies 2100 Bioanalyzer. Whole-genome root transcript profiling was performed using the maize 46K arrays obtained from the maize oligonucleotide array project (http://www.maizecdna.org/outreach/resources.html). Transcript abundance in each of the three replicates for vegetative and mature roots at low (N^-) and high (N^+) N supply was determined using a mixture of all the samples (12 in total, each with the same mRNA concentration) as a reference. Hybridizations between the maize oligonucleotide microarrays and fluorescently labeled samples were performed in MICROMAX Hybridization Buffer III (Perkin Elmer) using the manufacturer's hybridization and wash conditions and a GeneTac™ HybStation (Genomic Solutions, Ann Arbor, MI, USA). Before hybridization, 50 pmol Cy3- and 50 pmol Cy5-labeled targets were mixed, dried using compressed air, and reconstituted with 115 μl of hybridization buffer, followed by denaturing at 90 °C for 3 min. Each hybridization mixture was placed on maize 45K array slides mounted in the hybridization station and the hybridizations were performed for 3 h at 65 °C, followed by 3 h at 55 °C, then 12 h at 50 °C with gentle agitation. Thereafter, the arrays were automatically washed with the GeneTac™ washing solutions (Genomic Solutions) using the program for multiple automatic washes, with a flow time of 40 s. Immediately after the completion of the final washing step, the arrays were removed from the station, briefly immersed in distilled water, and air-dried with ozone-safe dry air. Hybridized microarrays were scanned using a GenePix 4000B Microarray Scanner (Molecular Devices, Sunnyvale, CA, USA) at 10 μm resolution and variable photomultiplier (PMT) voltage to obtain maximal signal intensities with <0.05% probe saturation. Subsequent image analysis was performed with the GenePix Pro (v6.0.1.26) software. Analysis included defining the spots, measuring the intensities, flagging spots when inadequate quality control parameters were found, and evaluating local background. The resulting files, containing all the scan data, were further processed using the statistical programming language R (http://www.r-project.org) together with the packages of the MAnGO project (Version 0.9.7, Microarray Normalization tool of GODMAP, CNRS BioInfome Team). The background level was calculated using morphological operators (a short closing followed by a large opening) and subtracted. Raw data were normalized using a global loess method. Gene annotation was provided by the maize oligonucleotide array project mentioned above (http://www.maizecdna.org/outreach/resources.html).

Statistical analysis of maize cDNA microarray data

Statistical group comparisons were performed using multiple testing procedures to evaluate statistical significance for differentially expressed genes. Two gene selection approaches were applied, namely the Significance Analysis of Microarrays permutation algorithm, and a *P*-value ranking strategy using both *z*-statistics in ArrayStat 1.0 software (Imaging Research Inc.) and moderated *t*-statistics using a moderated *t*-test available in MAnGO tools (Marisa *et al.*, 2007) and BRBArrayTools v3.2.3 packages. For multiple testing corrections, the false discovery rate (FDR) procedure was used. Statistical tests were computed and combined for each probe set using the log-transformed data, and a probe set was declared to be significant when the adjusted *P*-value was less than

the effective α-level (α=0.05) in at least one of these tests. A filtering procedure additionally excluded those data points considered biologically unreliable due to low signal intensities (A_{mean} <7.0). Transcriptomic data were validated by quantitative real-time reverse transcription–PCR (qRT–PCR) analysis performed on a selected number of gene transcripts up- or down-regulated. The validation process is shown in Fig. 1.

Metabolite extraction and analyses

Frozen maize root previously stored at –80 °C was used for the extraction of metabolites. A 100 mg aliquot of the root powder was placed in 1 ml of 80% ethanol/20% distilled water for 1 h at 4 °C. During extraction, the samples were continuously agitated and then centrifuged for 5 min at 15 000 rpm. The supernatant was removed, and the pellet was subjected to a further extraction in 60% ethanol and finally in water at 4 °C. All supernatants were combined to form the aqueous alcoholic extract. Total N content of 25 mg of frozen root material was determined in an elemental analyzer using the combustion method of Dumas (Flash 2000, Thermo Scientific, Cergy-Pontoise, France).

Metabolome analysis

All steps were adapted from the original protocol (Fiehn, 2006) following the procedure described in the literature (Amiour *et al.*, 2012). All extraction steps were performed in 2 ml Safelock Eppendorf tubes. The ground frozen root samples were resuspended in 1 ml of frozen (–20 °C) water:chloroform:methanol (1:1:2.5) and extracted for 10 min at 4 °C with shaking at 1400 rpm in an Eppendorf thermomixer. Insoluble material was removed by centrifugation, and 900 µl of the supernatant were mixed with 20 µl of 200 µg ml^{-1} ribitol in methanol. Water (360 µl) was then added and, after mixing and centrifugation, 50 µl of the upper polar phase were collected and dried for 3 h in a Speed-Vac and stored at –80 °C. Four blank tubes were subjected to the same steps as the samples. For derivatization, samples were removed from –80 °C storage, warmed for 15 min before opening, and Speed-Vac dried for 1 h before the addition of 10 µl of 20 mg ml^{-1} methoxyamine in pyridine. The reactions with the individual samples, blanks, and amino acid standards were performed for 90 min at 28 °C with continuous shaking in an Eppendorf thermomixer. A 90 µl aliquot of *N*-methyl-*N*-trimethylsilyl-trifluoroacetamide (MSTFA) was then added and the reaction continued for 30 min at 37 °C. After cooling, 50 µl of the reaction mixture were transferred to an Agilent vial for injection. For the analysis, 3 h and 20 min after derivatization, 1 µl of the derivatized samples was injected in the Splitless mode onto an Agilent 7890A gas chromatograph coupled to an Agilent 5975C mass spectrometer. The column used was an Rxi-5SilMS from Restek (30 m with a 10 m Integra-Guard column). The liner (Restek # 20 994) was changed before each series of analyses and 10 cm of the column were removed. The oven temperature ramp was 70 °C for 7 min, then 10 °C min^{-1} up to 325 °C, which was maintained for 4 min. Overall the total run time was 36.5 min. A constant flow of helium was maintained at 1.5231 ml min^{-1}. Temperatures in the gas chromatograph were the following: injector, 250 °C; transfer line, 290 °C; source, 250 °C; and quadrupole, 150 °C. Samples and blanks were randomized. Amino acid standards were injected at the beginning and end of the analyses for monitoring of the derivatization stability. An alkane mix (C10, C12, C15, C19, C22, C28, C32, C36) was injected in the middle of the analyses for external retention index calibration. Five scans per second were acquired. For data processing, Raw Agilent datafiles were converted into the NetCDF format and analyzed with AMDIS (https://chemdata.nist.gov/dokuwiki/doku.php?id=chemdata:amdis). A home retention indices/mass spectra library built from the NIST, Golm, and Fiehn databases and standard compounds was used for metabolite identification. Peak areas were then determined using the quanlynx software (Waters) after conversion of the NetCDF file into the masslynx format. Statistical analyses were carried out with TMEV (https://mev.tm4.org/). Univariate analyses by permutation (one- and two-way ANOVA) were first used to select the metabolites exhibiting significant changes in their concentration.

Model reconstruction

The primary set of reactions $J_{Primary}$ [1751 reactions from a combination of gene, protein, and reaction information from available public databases such as the Kyoto Encyclopedia of Genes and Genomes (KEGG; Kanehisa *et al.*, 2014), UniProt (Bateman, 2019), and MaizeCyc (Monaco *et al.*, 2013)], vascular tissue transporters (V_t; 43 transporters), and nutrients $J_{Nutrients}$ (eight nutrient sources) supplied to maize root were combined to form the draft model for maize root. Genes with an expression level above the cut-off defined by Downs *et al.* (2013) (i.e. 7.644) were categorized as highly expressed. Genes that were expressed at a level below the cut-off were categorized as expressed at a low level. When building the maize root model, the nutrients included those from the soil and those metabolites that can be imported from the vascular tissue. Inactive reactions, determined by using the gene expression data and GPR associations, were placed into a set termed $J_{Inactive}$ (72 reactions). Finally, spontaneous reactions and reactions with a GPR relationship that only contain genes in the 'always expressed at a low level' set were placed into the set $J_{NotMeasured}$ (77 reactions). To ensure that the maize root biomass reaction was not blocked given the available nutrients, a GapFill step

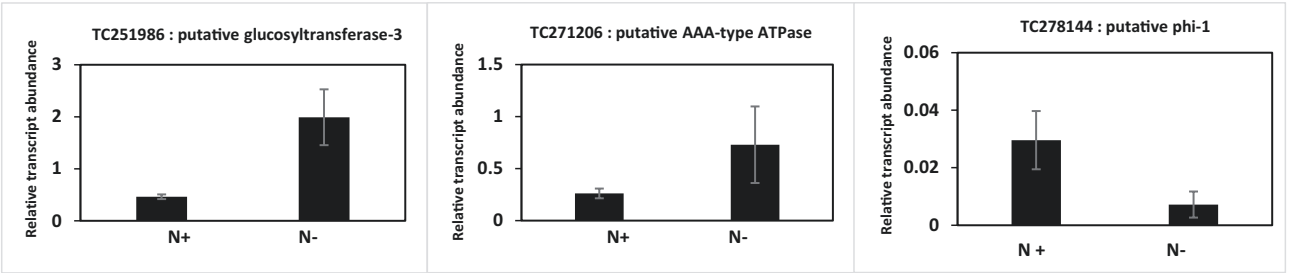

Fig. 1. Transcript abundance in roots of maize plants grown under N-limiting (N^-) and non-limiting conditions (N^+). Three N^--responsive genes were selected from the microarray experiment. Quantification of mRNA was performed using qRT–PCR. For the gene encoding a putative glucosyltransferase-3 (TC251986), the primers were F: GGGCTCCTGATTTCCACAA and R: TGCTACCTACCTCCCAACAACT. For the gene encoding a putative AAA-type ATPase (TC271206), the primers were F: GATGAGGAGAAAGGCAACGA and R: GCACTGCAAGTACCATTACACC. For the gene encoding a putative phi-1 (TC 278 144), the primers were F: CTGTCGGGATTGTGTAGCAA and R: CCGGTCCAACAAGTAACG. Each value was normalized with the relative transcript abundance of the gene encoding EF1a. Values are the mean ±SE of the three independent samples used for the microarray experiment. The *t*-test was 0.05 for TC251986 and TC278144, and 0.1 for TC271206.

(Satish Kumar *et al.*, 2007) was performed for the maize root. The following algorithm was used to determine the minimum number of reactions added with a preference for adding reactions from the not measured set over reactions in the inactive set (Equation 1):

$$\min \sum_{j \in J_{NotMeasured}} y_j + 10 \sum_{j \in J_{Inactive}} y_j$$

Subject to:

$$\sum_{j \in J} S_{ij} v_j = 0, \ \forall i \in I \quad [1]$$

$$LB_j \leq v_j \leq UB_j, \ \forall j \in J_{Primary} \cup J_{Nutrients} \cup V_t \quad [2]$$

$$LB_j y_j \leq v_j \leq UB_j y_j, \ \forall j \in J_{Inactive} \cup J_{NotMeasured} \quad [3]$$

$$v_{biomass} \geq 0.001 \quad [4]$$

Here S_{ij} is the stoichiometric coefficient of metabolite i in reaction j, and v_j is the flux through reaction j. Sets I and J include all metabolites and reactions known to occur within maize, respectively. The lower bound, LB_j, and upper bound, UB_j, of reaction j (Equations 2 and 3) are sufficiently small and large and are determined by each reaction's directionality based on thermodynamic constraints. The binary variable, y_j, is equal to 1 if the reaction is added to the model and 0 otherwise (Equation 3). Finally, a small amount of flux is forced through the biomass equations (Equation 4) to ensure biomass is not blocked. From this algorithm, a set of reactions, $J_{Secondary}$, was added to the maize root models to ensure that flux through the biomass reaction is possible.

A second GapFill step was performed to activate as many reactions in the primary set as possible for maize root. The GapFill algorithm displayed above was completed successively for each reaction that did not carry flux in the primary set by modifying the model constraints in the following manner. First, Equation 2 was extended to encompass the secondary set of reactions to account for their inclusion in the maize root model. Second, Equation 4 was applied to reactions of interest rather than the biomass reaction. Reactions from $J_{NotMeasured}$ were added as needed; however, reactions from $J_{Inactive}$ were only included in the final model if their addition allowed 10 previously blocked reactions from the active set to carry flux. This was done to ensure that reactions with genes that are expressed at a low level in the maize root based on transcriptomic data were added only if they allow for flux through multiple reactions in the primary set.

Eliminating thermodynamically infeasible cycles through flux variability analysis

To identify thermodynamically infeasible cycles in the model, FVA (Mahadevan and Schilling, 2003) was used by turning off all the nutrient uptakes to the cell. The formulation is as follows.

$$\max / \min \ v_j$$

Subject to:

$$\sum_{j \in J} S_{ij} v_j = 0, \ \forall i \in I \quad [5]$$

$$LB_j \leq v_j \leq UB_j, \ \forall j \in J \quad [6]$$

FVA maximizes and minimizes each of the reaction fluxes subject to mass balance and environmental, and any artificial (i.e. biomass threshold), constraints. The reaction fluxes which hit either the lower or upper bounds were defined as unbounded reactions, and were grouped as a linear combination of the null basis of their stoichiometric matrix. These groups are indicative of possible thermodynamically infeasible cycles. To eliminate the cycles, duplicate reactions were removed, lumped reactions were turned off, or reactions were selectively turned on/off based on available cofactor specificity information. In this study, FVA was also used to find the flux ranges/flux variability of different reactions.

Incorporation of transcriptomics data with the model through E-Flux

E-Flux is an extension of FBA that uses transcriptomic data to impose upper and lower bounds on reaction fluxes (Colijn *et al.*, 2009; Brandes *et al.*, 2012). The rationale behind E-Flux is that, given a limited translational efficiency and a limited accumulation of enzyme over time, the mRNA level can be used as an approximate upper bound on the maximum number of metabolic enzymes, and hence corresponding reaction rates. The E-Flux algorithm offered the flexibility to constraint the reaction flux based on the association of gene expression with the GPR. In addition, in contrast to other transcriptomics data integration methods, the E-Flux algorithm utilizes a metabolic network model to directly predict changes in reaction flux, hence resulting in improved prediction of reaction fluxes under N^+ and N^- condition. The standard FBA involved solving the following linear optimization problem:

$$\max \ v_{biomass}$$

Subject to:

$$\sum_{j \in J} S_{ij} v_j = 0, \ \ \forall i \in I \quad [7]$$

$$a_j \leq v_j \leq b_j \quad [8]$$

where vector v represents a particular flux configuration, S is the stoichiometric matrix, and a_j and b_j are the minimum and maximum allowed fluxes through reaction j. It was assumed that a set of expression measurements for some or all of the genes associated with the reactions in S were available. The E-Flux method calculates the upped bound, b_j, for the jth reaction according to the following function of the gene expression:

$$b_j = (\exp \textit{ression level of genes associated with reaction } j) \quad [9]$$

In this study, b_j is the exact level of each reaction that was calculated through its GPR association [i.e. based on the 'OR' (addition of gene expressions) and 'AND' (minimum of gene expressions) relationship]. If the reaction catalyzed by the corresponding enzyme was reversible then a_j=−b_j, otherwise a_j=0.

Metabolite pool size calculations through flux-sum analysis

Metabolite pool size were determined based on the flux-sum analysis (FSA) method (Chung and Lee, 2009). The flux-sum is a measure of the amount of flux through the reactions associated with either the production or consumption of the metabolite. The range of the flux-sum or the flow through of each metabolite with experimental measurements was maximized/minimized as follows:

$$\begin{bmatrix} Max/Min \ 0.5 \sum_{j=1}^{m} \left| S_{ij} v_j \right| & [10] \\ Subject \ to: & [11] \\ \sum_{j=1}^{m} S_{ij} v_j = 0, \ \forall i \in 1, \ldots, n & \\ v_{j,\min} \leq v_j \leq v_{j,\max} & [12] \\ v_{biomass} = v_{biomass}^{\max} & \end{bmatrix}, \forall i \in I_E$$

Here, set I_E represents the set of metabolites with experimental measurements. The formulation was run in an iterative manner for each metabolite with experimental measurements and repeated for both conditions.

By linearizing the objective function, the resulting formulation became a mixed-integer linear programming problem. FSA assumes that any biological system is under steady state (Equation 10) with specific bounds on the reaction fluxes (Equation 11). As a result, the aggregate reaction flux associated with productions and consumptions of a specific metabolite must be equal with an opposite sign. Hence, in the FSA, the objective function is the average of absolute values of both production and consumption reactions of a metabolite. The flux-sum ranges were determined at the maximum biomass for the condition as displayed in Equation 12. Predictions were made only when the flux-sum ranges did not overlap between the background condition and the condition to be compared. In this way, the compartment-specific predictions of the flux-sum ranges were compared with tissue-specific experimental measurements. As GSM is a steady-state model, diminishing or expanding the pool size based on fast or slow reaction kinetics is not a possibility here.

Fold change calculations

In FBA, reaction fluxes and optimal pathways are found by solving a linear optimization problem, in which usually the growth rate is maximized subject to pseudo-steady-state mass balance and other environmental constraints. However, degeneracy in metabolic networks leads to an infinite number of reaction flux distributions satisfying given constraints and the objective function. Moreover, some of these reaction flux distributions may bear no or incorrect biological relevance for a given condition. To avoid this, while calculating *in silico* fold change (metabolite pool size in N^-/metabolite pool size in N^+) of metabolites, FSA was used to generate a range (minimum and maximum) of metabolite pool size, in both N^- and N^+ conditions. In this study, *in silico* fold change is a qualitative idea, where the flux range of a specific metabolite under N^- condition is compared with that of the same metabolite under N^+ conditions. Hence, we only determined *in silico* fold change for metabolites if flux-sum variabilities in these conditions do not overlap with each other. That leads *in silico* fold change to assume only three qualitative values—overlap, increase, and decrease (see Table 1 for details).

Once the compartment-specific *in silico* fold change of metabolites was calculated, these fold changes were compared with the experimental metabolomics data-based fold changes which were measured for the whole cell.

Use of the BLASTp algorithm to find homologous genes

Arabidopsis gene sequence data were obtained from the TAIR database (http://www.arabidopsis.org/). To identify Arabidopsis gene homologs in maize, systematic bidirectional BLASTp (https://blast.ncbi.nlm.nih.gov/Blast.cgi?PAGE=Proteins) searches were performed against the NCBI non-redundant database using the sequences of Arabidopsis genes. The screening criterion was E-value 10^{-10}. In the case of multiple homologous genes for maize, genes were chosen based on the higher Max score.

Simulation software

The General Algebraic Modeling System (GAMS) version 24.7.4 with IBM CPLEX solver was used to run FBA and FVA, E-Flux, and the FSA algorithm on the model. Each of the algorithms was scripted in GAMS and then run on a Linux-based high-performance cluster computing system at the University of Nebraska-Lincoln.

Results and discussion

Development and validation of the maize root model

A GSM of maize root was reconstructed using a combination of gene, protein, and reaction information from available public databases such as KEGG (Kanehisa *et al.*, 2014), UniProt (Bateman, 2019), and MaizeCyc (Monaco *et al.*, 2013). The draft model was curated as described in the Materials and methods. Figure 2 shows how model reconstruction and refinement were carried out. The model also included the metabolites that are transported through the phloem and xylem tissues supported by literature evidence (Yesbergenova-Cuny *et al.*, 2016). The phloem and xylem tissues were combined, for simplicity, in the model and are referred to as the vascular tissue. Specific pathways such as the sphingolipid pathway, benzoxazinoid pathway, linoleic acid pathway, β-alanine pathway, and flavonoid biosynthesis were introduced based on genomic annotation and experimental evidence from the literature as described in the subsequent sections. The reconstructed model contains 6389 genes, 4002 reactions, and 4461 metabolites distributed across six intracellular compartments, namely the cytosol, plastid, mitochondria, peroxisome, plasma membrane, vacuole, and inner mitochondrial matrix. Biomass accumulation is represented in the metabolic model by a root-specific biomass assuming that the biomass composition does not change across different environmental conditions. Within the biomass reaction, the stoichiometric coefficients represent the proportion of each biomass component ensuring that the overall biomass molecular weight is 1 g mol^{-1} for proper component balance (Chan *et al.*, 2017). Growth- and non-growth-associated ATP maintenance levels were based on available measurements for maize root (Roberts *et al.*, 1985; Doncheva *et al.*, 2006).

In order to validate the model and to ensure that it could simulate biologically relevant situations, a case study involving strigolactones was selected. Strigolactones, a group of carotenoid-derived terpenoid lactones, can regulate root architecture and act as phytohormones and rhizosphere signals (Guan *et al.*, 2012; Walton *et al.*, 2016). Strigolactones also promote the elongation of seminal/primary roots and adventitious roots, and they repress lateral root formation (Sun *et al.*, 2016). Given the importance of strigolactones, the key question was if the maize root model could recapitulate the manifestation

Table 1. Three different cases of *in silico* fold change under N^- and N^+ conditions for a fictitious metabolite A

Cases	Metabolite pool size (N^-)	Metabolite pool size (N^+)	Decision
Case 1	[0.50 0.75]	[0.25 0.60]	Overlap in flux-sum variability: indeterminate fold change.
Case 2	[0.60 0.75]	[0.25 0.50]	No overlap in flux-sum variability: increased fold change.
Case 3	[0.15 0.25]	[0.35 0.60]	No overlap in flux-sum variability: decreased fold change.

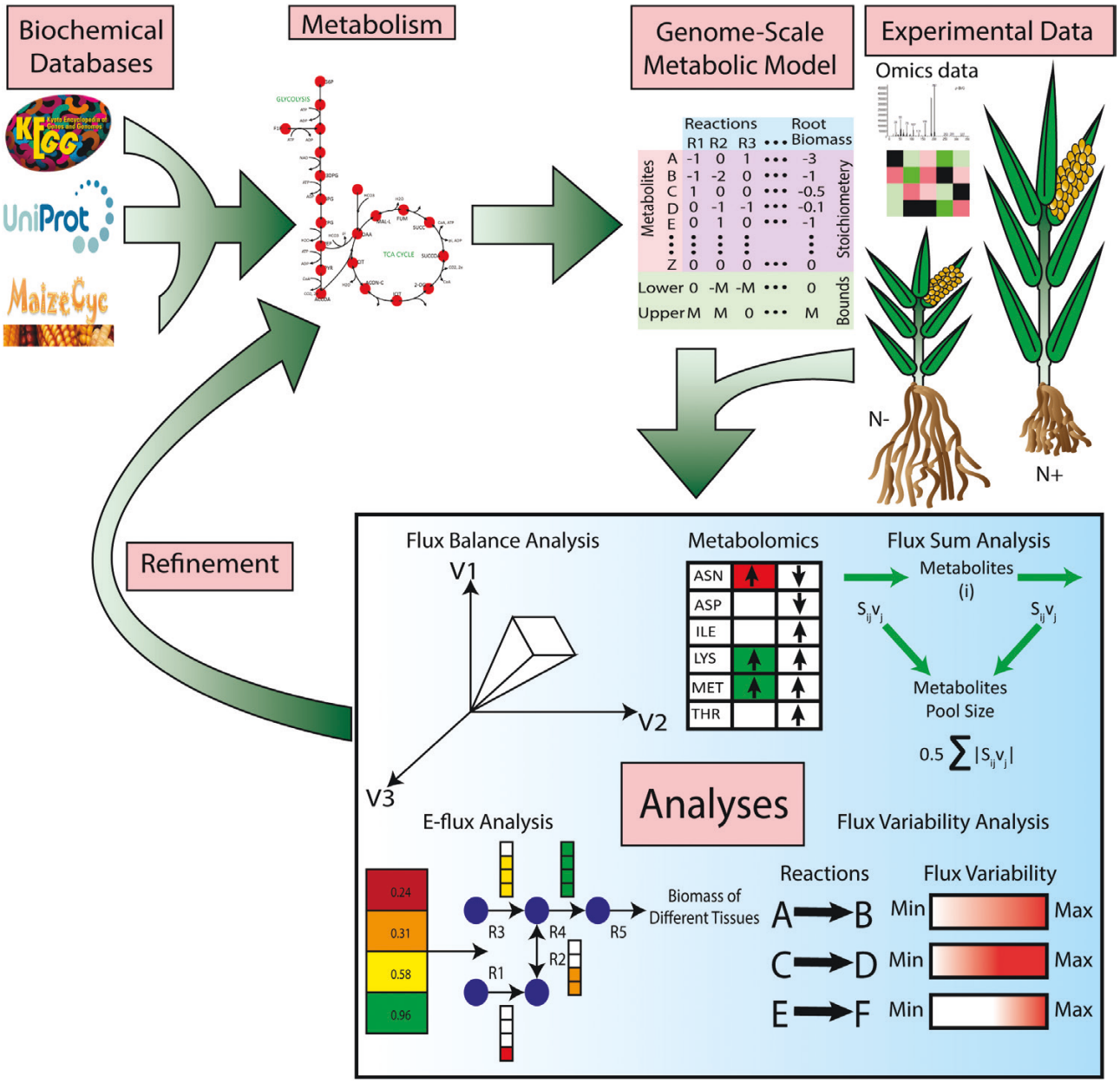

Fig. 2. This figure demonstrates the overall process of the model development and refinement. From different biochemical databases such as KEEG, UniProt, and MaizeCyc, the maize root metabolic pathway was reconstructed. From that reconstructed maize root metabolic pathway, a genome-scale metabolic model was developed. Experimental omics data for nitrogen optimal (N^+) and nitrogen starvation condition (N^-) were then integrated with the model to analyze metabolic reprogramming of maize root under N^-. Different techniques, such as flux balance analysis (FBA), flux-sum analysis (FSA), the E-Flux algorithm, and flux variability analysis (FVA) were used to analyze the model and come up with different findings of this study. The maize root genome-scale metabolic model can be found in Supplementary Table S1. Experimental transcriptomics and metabolomics data can be found in Supplementary Table S2.

of these effects in terms of metabolic changes. To the best of our knowledge, no large-scale combined transcriptomics and metabolomics data are available for maize root to adequately constrain the model. Thus, the relevant information was gathered from a study performed in *A. thaliana* (Walton *et al.*, 2016) in which the impact of the strigolactone analog *rac*-GR24 was elucidated on the root proteome of the wild type (WT) and the signaling mutant *more axillary growth 2* (*MAX2*). The study revealed a clear *MAX2*-dependent *rac*-GR24 response, which indicated an increase in abundance of enzymes involved in flavonol biosynthesis. This abundance of enzyme in flavonol biosynthesis was reduced in the *max2-1* mutant. Details of the experimental design and screening of these genes can be found in the original paper (Walton *et al.*, 2016). To identify

the homologous genes encoding the corresponding proteins in maize, a bidirectional BLASTp search was conducted. Later, the abundance of those proteins was used to incorporate reaction flux regulations via GPR in the maize root model using the E-Flux algorithm for predicting the response of the maize root to the synthetic strigolactone *rac*-GR24.

As the number of homologous genes with measured protein levels was low, most of the metabolic pathways between the WT and *rac*-GR24-stimulated maize root showed similar flux ranges, found using FVA. However, the maize root model was able to predict the reduced reaction flux through the flavonoid biosynthesis and the phenylpropanoid pathways, similar to what was inferred in the original study (Walton *et al.*, 2016). Walton *et al.* reported a reduction of concentration of flavanone, *p*-coumaroyl hexose, quercetin glucoside, naringenin, and kaempferol glucoside for the *max2-1* mutant. Through flux-sum variability analysis, a representative of the steady-state metabolite pool size, the maize root model also predicted shrinkage of metabolite pool sizes of these particular metabolites. In addition, through FBA, the model predicted reduced flux in the metabolism of some amino acids such as valine–leucine–isoleucine metabolism, alanine–aspartate–glutamate metabolism, arginine metabolism, phenylalanine–tyrosine–tryptophan metabolism, and cysteine–methionine metabolism of maize root. 2,4-Dihydroxy-7-methoxy-1,4-benzoxazin-3-one-glucoside (DIMBOA-glucoside) production in the benzoxazinoid pathway also showed decreased flux. DIMBOA is a tryptophan-derived heteroaromatic metabolites with benzoic acid moieties that are produced in large quantities by maize roots (Cotton *et al.*, 2019). Previous studies have shown that benzoxazinoids and their breakdown products are biocidal to some soil-borne pathogenic bacteria and fungi (Cotton *et al.*, 2019). Hence, the lack of strigolactones in maize roots may result in weaker defense against some soil-borne pathogens. In addition, galactose metabolism, glutathione metabolism, and purine metabolism showed reduced flux. Interestingly, steroid metabolism in the *rac*-GR24-simulated maize root showed increased flux which can usually be linked to plant growth, reproduction, and responses to various abiotic and biotic stresses (Vriet *et al.*, 2012). The validation study is summarized in Fig. 3 .

Improved model predictions through incorporation of omics data

In order to accurately model N deficiency, transcriptomics and metabolomics datasets were generated from the maize plants grown in a hydroponic system under N^- and N^+ conditions. These transcriptomics data were incorporated into the root model, using the E-Flux algorithm, to study metabolic reprogramming of the maize root under N^- condition Before the integration of transcriptomics data, the FBA predicted a 21% reduction of biomass in N^- compared with N^+ conditions, whereas upon the integration of transcriptomics data the trend reversed (with a 285% increase in N^- condition). For maize, it was reported that low N content in the growth medium increased primary root growth at the vegetative state (Mager and Ludewig, 2018). In N^- condition, roots tend to go deeper into the medium to scavenge more N (Cai *et al.*, 2012). The increased growth of the root in N^- condition comes at the expense of decreased shoot growth (Mardanov *et al.*, 1998; Puig *et al.*, 2012). Similar root growth behavior in N^- condition was observed in other plants including *A. thaliana* (Oldroyd and Leyser, 2020) and *O. sativa* L. ssp. *japonica* (Cai *et al.*, 2012).

To gather further inferences on the increased root biomass production in N^- condition, flux-sum variability analysis for all the biomass metabolites was performed. Except for lipids of glycerolipid metabolism, all other metabolites showed an increased but non-overlapping metabolic pool size under N^- condition (Fig. 4). To further investigate the flux-sum variability of those lipid metabolites under N^- condition, biomass production in the model was fixed between its minimum and maximum values. With the reducing biomass growth, the flux-sum ranges of different lipid metabolites in N^- condition approached the corresponding flux-sum ranges in N^+ conditions, When the biomass production under N^- was fixed to the biomass production in N^+, most of the lipids showed similar flux-sum variability ranges to those in N^+ except for 160PC (16:0 phosphatidylcholine), 160PG (16:0 phosphatidylglycerol), 181PC (18:1 phosphatidylcholine), 181PG (18:1 phosphatidylglycerol), 182PC (18:2 phosphatidylcholine), 182PG (18:2 phosphatidylglycerol), 183PC (18:3 phosphatidylcholine), and 183PG (18:3 phosphatidylglycerol). To investigate these eight metabolites further, flux-sum variability was conducted for N^- with zero biomass requirement, which revealed zero flux-sum for all the phosphatidyl metabolites except for those eight metabolites. These eight types of lipids were unlikely to be coupled with either an increase or a decrease in biomass production under N^- and N^+ conditions. Among those lipids, four of them (160PG, 181PG, 182PG, and 183PG) do not contain any nitrogen, while the rest contain nitrogen. A close observation of the glycerolipid metabolism pathway revealed that *S*-adenosyl-L-methionine from cysteine–methionine metabolism and citicoline from glycerophospholipid metabolism are the precursors of these four metabolites. *S*-Adenosyl-L-methionine is directly produced from L-methionine, and the flux-sum variability comparison with the metabolomics data revealed an increased fold change of L-methionine in the N^- condition. Citicoline is produced from the choline phosphate in glycerophospholipid metabolism and exhibited a widened reaction flux under N^-. Hence, increased fold change of L-methionine and widened reaction flux for citicoline production played an important role in elevated flux-sum ranges of 160PC, 181PC, 182PC, and 183PC in N^- condition.

After investigating biomass production in both conditions, the increasing or decreasing trend of metabolite content in N^- with respect to that measured in N^+ was qualitatively

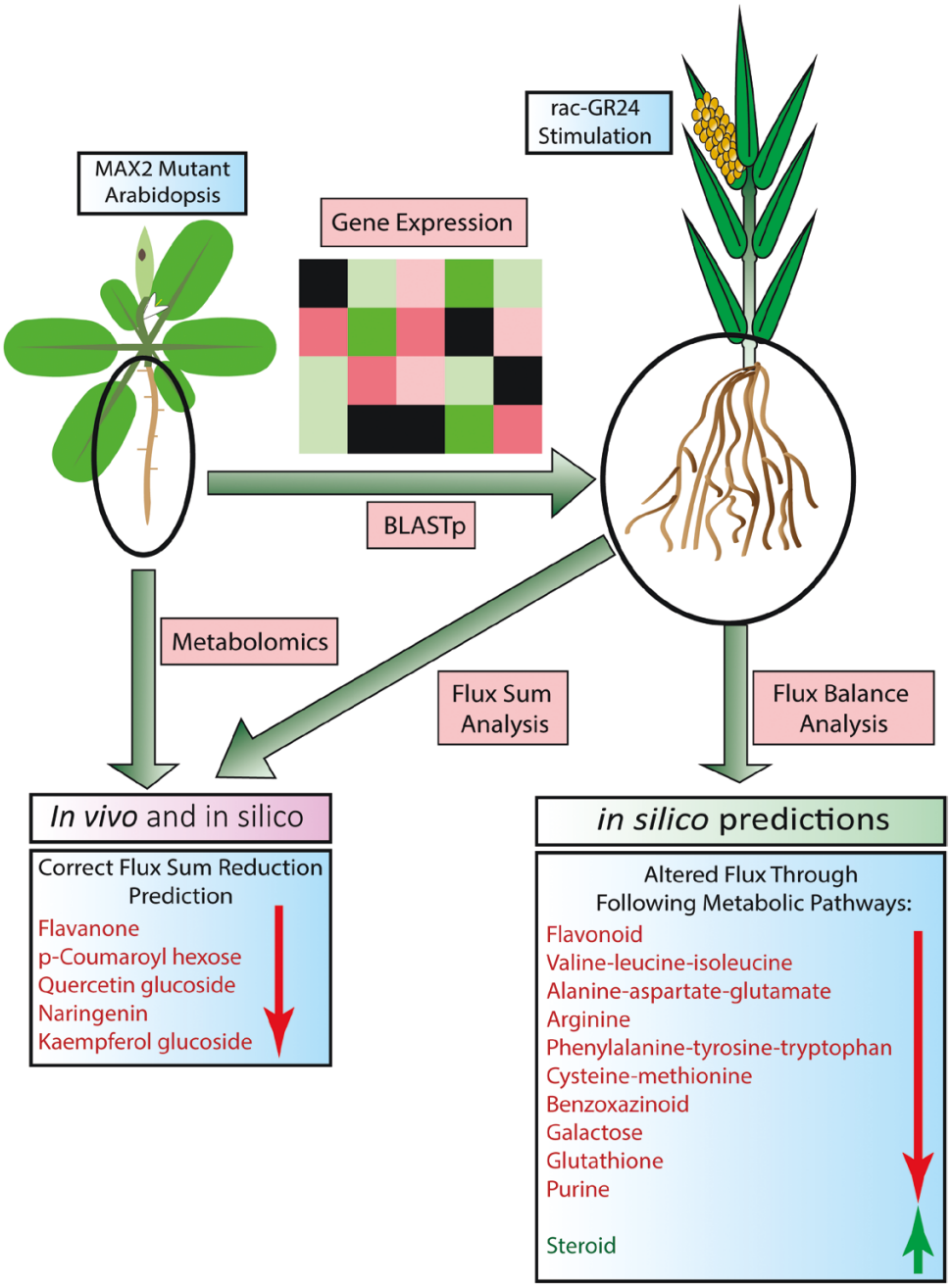

Fig. 3. Summary of validation of the maize root GSM on the effect of strigolactone on maize root. The gene expression from the *MAX2* mutant of Arabidopsis root was projected to maize root through a homologous BLASTp search to simulate the effect of the strigolactone analog rac-GR24. Then gene expression data were integrated with the maize root model. *In silico* predictions from that model are shown in the right panel of the figure. Later, flux-sum analysis (FSA) was used to calculate the metabolic pool size for specific metabolites under both examined and base conditions. Those flux-sums were used to calculate the *in silico* fold change and those *in silico* fold changes were compared with the experimental metabolomics fold change data. The result is presented in the left table. Detail information regarding each step of validation can be found in Supplementary Table S3.

compared with the changes in the flux-sum ranges, a representative of steady-state metabolite pool size, as determined by the model. To this end, a flux-sum variability analysis was performed, and the flux-sum ranges that did not overlap between these conditions were analyzed. A correct prediction is one where the fold change occurs in the same direction computationally as well as in the experimental data, whereas an incorrect prediction is the one where the fold change occurs in opposite directions. An increase/decrease in the flux-sum of a metabolite between the N^- and the N^+ conditions was compared with the changes in metabolite concentration. After integration of transcriptomics data, the model was able to

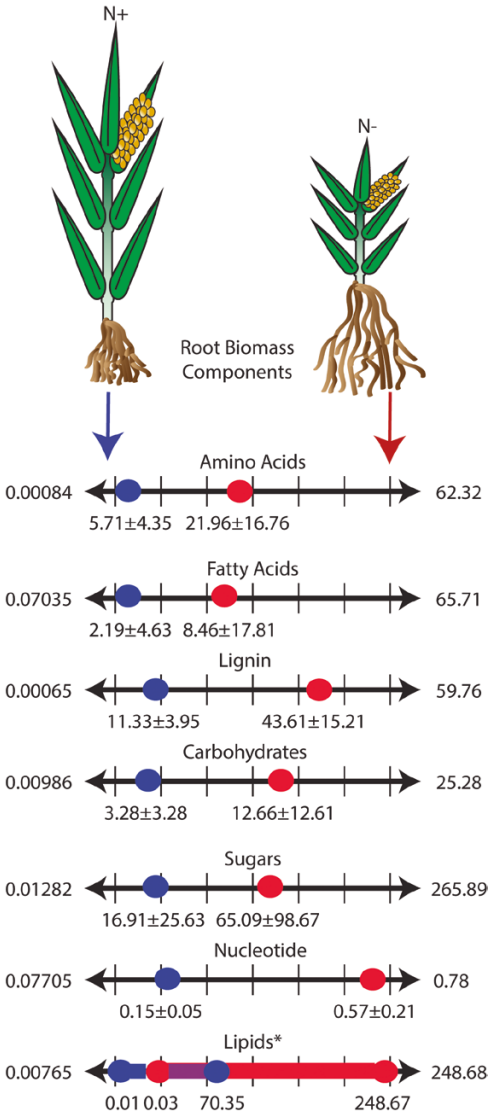

Fig. 4. A quantitative depiction of the flux-sum variability of different biomass components under N^- and N^+ conditions assuming maximization of biomass production. Supplementary Table S2 contains the full list of biomass precursors including references. Flux-sum variability of amino acids, fatty acids, lignin, carbohydrates, sugar, and nucleotides shrunk to a point, while only for lipids did the flux-sum variability show an overlapping range. For amino acids, fatty acids, lignin, carbohydrates, sugars, and nucleotides, each dot represents an average flux-sum value with an SD. *Detailed analysis of lipid metabolism and quantitative flux-sum variability for all the biomass components are presented in Supplementary Table S4.

predict increased fold changes of metabolites between the N^- and N^+ conditions. Metabolomics information was available for 73 metabolites, distributed over different compartments; out of those 73 metabolites, the model was able to predict fold change for 30 metabolites (41.1%). All these 30 metabolites exhibited an increased fold change. The rest of the 43 metabolites had overlapping flux-sum variability and the model could not predict their *in silico* fold changes. Figure 5 demonstrates the importance of incorporating transcriptomic data as additional parameters in the model. In N^- condition, the accuracy (the ratio of correct prediction after omics data integration and before omics data integration) increased by >10-fold when the flux constraints based on transcriptomics data were incorporated to the model.

Among the metabolites for which fold change was predicted, five metabolites (L-lysine, glycerol-3-phosphate, glycerol, L-asparagine, and linoleic acid), were common both before and after the integration of transcriptomics data. Of these metabolites, increased fold change of L-lysine was correctly predicted by the model only after integration of transcriptomics data. For L-asparagine, the model prediction of increased fold change was correct after the integration of transcriptomics data. For the three other metabolites, the prediction remained incorrect both before and after the integration of transcriptomics data. L-Asparagine is widely known as a major nitrogen carrier in plants in a number of key biological processes such as germination, vegetative growth, senescence, and seed filling. Initially in the model, both the root biomass and the pool size of L-asparagine were higher in N^+ compared with N^- condition. Furthermore, after incorporation of transcriptomics data,

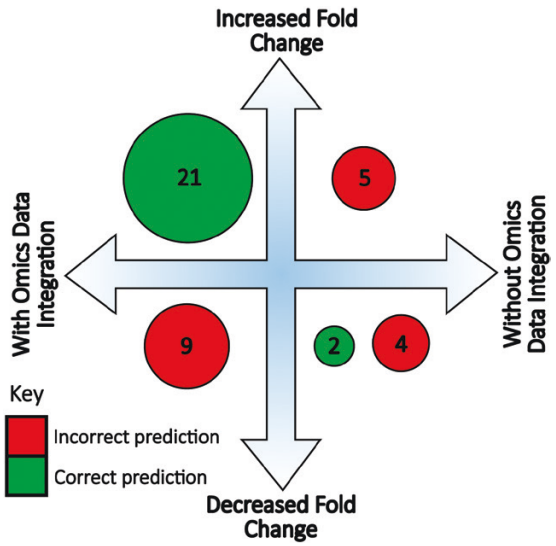

Fig. 5. Effect of omics-based data integration on the flux-sum prediction compared with the experimental trend in metabolite concentration. The accuracy in predicting the increasing (up arrow) or decreasing (down arrow) trend in metabolite change between N^+ and N^- is displayed. The top left corner of the figure represents the correct/incorrect prediction with increased fold change after the integration of omics data. The bottom left corner of the figure represents the correct/incorrect prediction with decreased fold change after the integration of omics data. The top right corner of the figure represents the correct/incorrect prediction with increased fold change before the integration of omics data. The bottom right corner of the figure represents the correct/incorrect prediction with decreased fold change after the integration of omics data. Before integration of omics data, there were two correct predictions, nine incorrect predictions, and 62 metabolites had an overlap of the flux-sum range. After integration of omics data, there were 21 correct predictions, nine incorrect predictions, and 43 metabolites had an overlap of the flux-sum range.

both parameters were predicted to be higher in N^- condition. Hence, the model predicted that the pool size of L-asparagine is one of the key indicators for predicting root biomass production in N^-. Such an accumulation of L-asparagine was also observed under other abiotic stress conditions in wheat (Naidu *et al.*, 1991; Oddy *et al.*, 2020), *Coleus* (Gilbert *et al.*, 1998), and barley (Yamaya and Matsumoto, 1989).

Before integration of transcriptomics data, the decreased fold change of glycine in N^- was correctly predicted. Following the integration of transcriptomics data, the flux-sum range of glycine in N^+ and N^- condition overlapped with each other. In this study, we found that glycine translocation in the root through vascular tissues played an important role in this overlap. If we refer to the work of Yesbergenova-Cuny *et al.* (2016), it has been found that glycine and arginine each represented 3% of the total phloem sap amino acid content. Thus, under N^-, once the flux of glycine through vascular tissue was set to 85% of that of arginine, we observed that the metabolite pool size of glycine no longer overlapped between the N^+ and the N^- condition, leading to a correct decreased fold change prediction from the model after transcriptomics data integration. Glycine is thus an example for which transcriptomics data integration in the model can lead to erroneous flux prediction.

By incorporating transcriptomics data, the fold change in the content of several key components of the tricarboxylic acid (TCA) cycle such as 2-oxoglutarate, succinate, fumarate, and malate were correctly predicted. 2-Oxoglutarate is a key intermediate of the TCA cycle as it is the main provider of the C skeleton to the ammonium assimilatory pathways leading to the synthesis of glutamine and glutamate (Huergo and Dixon, 2015). Other metabolites of the TCA cycle, such as succinate, play an important role during the process of symbiotic atmospheric N_2 fixation (Flores-Tinoco *et al.*, 2020), whereas fumarate works as a C sink for both phenylalanine and tyrosine in higher plants (Hockin *et al.*, 2012). In root nodules, malate is the primary substrate for bacteroid respiration, providing energy to sustain the activity of the nitrogenase enzyme and thus the rate of N_2 fixation. Furthermore, the fold changes of several key amino acids such as lysine, arginine, methionine, cysteine, leucine, histidine, and valine that are essential for plant growth and development were correctly predicted by the model (Fig. 6). In addition, the model predicted an increase in the cholesterol and L-pipecolate contents, both being key components of root biomass production, notably under N^- condition. Overall, following integration of transcriptomics data, true prediction of metabolite fold change increased from 18% to 70%. In addition, the false prediction rate of metabolite fold change decreased from 82% to 30%.

Besides these correct predictions, fold changes for *O*-acetyl-L-serine and urea, both having decreased experimental fold change, were predicted incorrectly by the model even after the integration of transcriptomics data. For these two metabolites, flux-sum range overlapped between the N^- and N^+ conditions, leading to the impossibility to predict changes in their content before transcriptomic data integration. Even after transcriptomic data integration, we were not able to correctly predict changes in their abundance. Although we found that *O*-acetyl-L-serine was predominantly transported from leaves to the roots and that a minimum flux of *O*-acetyl-L-serine was necessary to sustain maximum biomass production in N^- condition, the model prediction remained incorrect. A similar situation occurred for urea, where at maximum biomass production, when the reaction flux of arginine to urea production was reduced by 50%, the model prediction was still incorrect. Missing pathways or reactions, lack of regulatory constraints, and inadequate flow regulations through the vascular tissue under N^- condition could explain why these predictions were incorrect.

Flux range variations under nitrogen stress condition in a hydroponic system reveal important metabolic reprogramming

Upon confirming that the model can capture the aggregate metabolic variations, we investigated the metabolic reprogramming under N^- using FVA. To this end, assuming that root biomass is maximized, the flux range of a specific reaction in N^- was compared with the flux range in N^+ in order to study the metabolic reprogramming under N^-.

The flux range of reactions in different metabolic pathways is shown in Fig. 7. Central C metabolism (CCM) plays an important role in the metabolic network and is composed of the flow of C from nutrients in the different cell types via the vascular tissues to build the important components of root biomass production. The main pathways of the CCM are glycolysis/gluconeogenesis, the pentose phosphate (PP) pathway, and the TCA cycle. Figure 6 shows how different metabolites from these pathways work as precursors for several biomass components. In glycolysis, the linear pathway from glyceraldehyde-3 phosphate to acetyl-CoA showed an elevated reaction flux except for the shrinkage in the reaction flux for the interconversion between glyceraldehyde-3 phosphate and glycerone phosphate. In the PP pathway, breakdown of ribose-5 phosphate to ribose, glycerate-3 phosphate production from glyceraldehyde-3 phosphate, and production of gluconate-6 phosphate from glucose-6 phosphate exhibited widened reaction flux. In the TCA cycle, most of the reactions showed a widened reaction flux which was consistent with the experimental metabolomics data and metabolite pool size calculations shown in Fig. 6. In order to have a perspective on the energy metabolism, flux-sum variability analysis of ATP was performed showing that its increase in N^- condition was well correlated with these increased fluxes through the TCA cycle. Since CCM metabolites work as precursors to produce molecules that play a seminal regulatory role under abiotic stress conditions, in the following sections we will discuss metabolic reprogramming of different pathways under N^- condition.

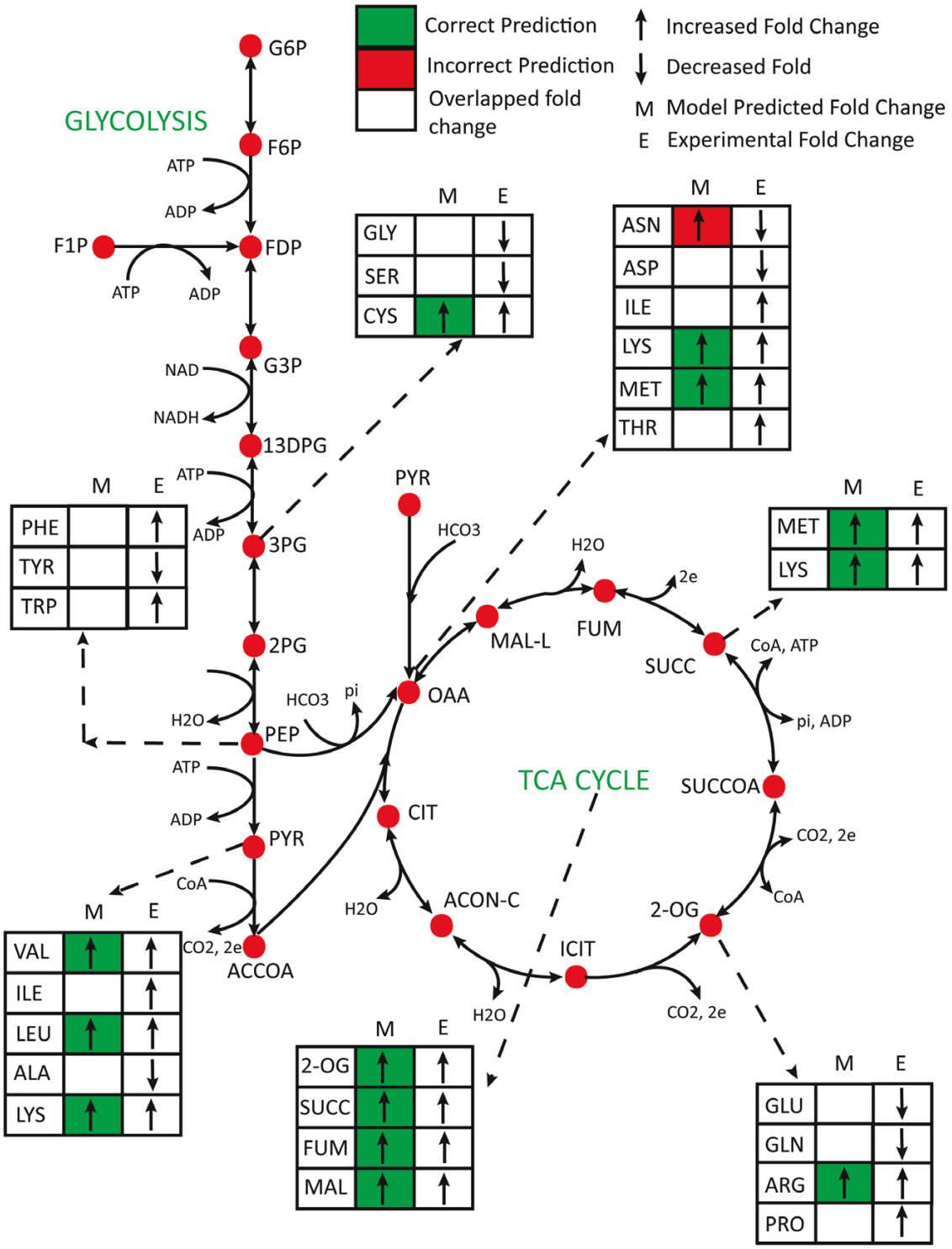

Fig. 6. Prediction from the model for the production of carbon skeletons and the subsequent synthesis of key amino acids in central carbon metabolism. On each panel, the first column with a letter indicates different amino acids or metabolites from the TCA cycle. M indicates the prediction from the model and E indicates the result from the experimental study. Upward arrows indicate an increased metabolic pool size of a metabolite in the N^- compared with the N^+ condition. Downward arrows indicate decreased metabolic pool size of a metabolite in N^- compared with N^+. The standard abbreviations for the different carbon and nitrogen metabolites were used. The flux-sum level in each condition can be found in Supplementary Table S5.

Plant sphingolipid metabolites have important roles as signaling molecules during both biotic and abiotic stresses (Ali *et al.*, 2018). Sphingolipid metabolism starts by combining L-serine and palmitoyl-CoA to produce 3-dehydro-D-sphinganine. Under N^- condition, the flux going through the reaction catalyzed by the sphingosine kinase enzyme, which

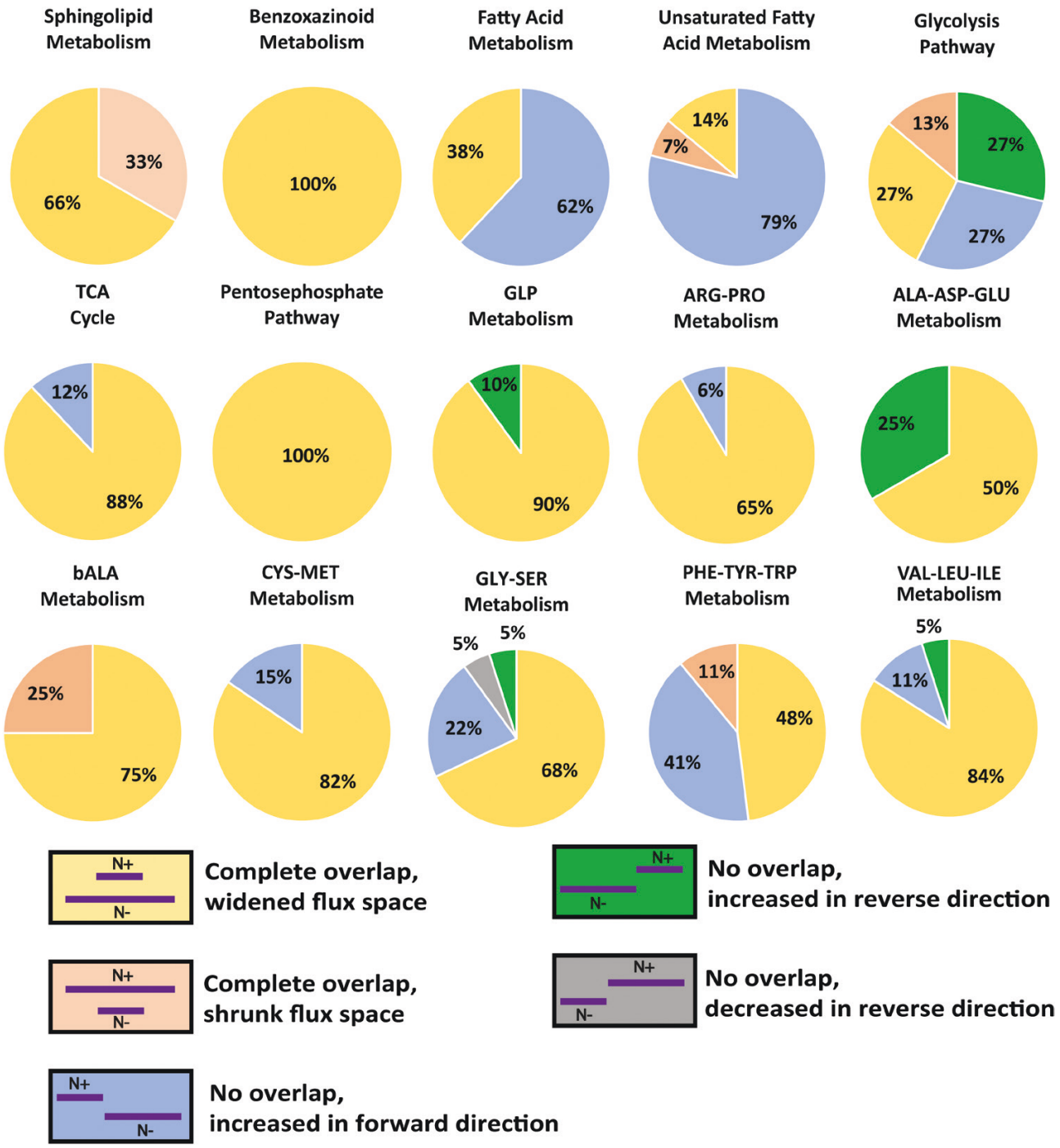

Fig. 7. Each pie chart represents metabolic reprogramming of a specific metabolic pathway with a N^+ base condition and N^- examined condition. Each component of the pie chart represents one of the five categories mentioned in the key. Each key shows how flux range of reactions change in the examined condition (N^-) compared with the base condition (N^+). The associated percentage in the pie chart represents the percentage of overall reactions of a specific pathway falling into each of the categories. Supplementary Fig. S1 shows a representation of the number of reactions in each category for a specific metabolic pathway.

produces sphingosine 1-phosphate, increased. Sphingosine 1-phosphate plays a critical role as a signaling molecule during different stress conditions, by regulating cell growth, and suppressing programmed cell death (Spiegel and Milstien, 2003). In contrast, the interconversion between lactosylceramide and glucosylceramide exhibited a reduced flux in N^- condition. Similar to sphingolipid metabolism, the reaction flux producing the final product of benzoxazinoid biosynthesis, DIMBOA, increased in N^- condition. DIMBOA acts as a signaling molecule to attract the plant growth-promoting rhizobacteria

Pseudomonas putida KT2440 (Niemeyer, 2009; Neal *et al.*, 2012; Costa-Gutierrez *et al.*, 2020). Such a signaling role could also be important during root growth in N^- condition.

In fatty acid metabolism, the concentration of triacylglycerol and free fatty acids increased in Arabidopsis under N^- (Gaude *et al.*, 2007). Fatty acid accumulation was also observed in other photosynthetic organisms such as *Chlamydomonas reinhardtii* (James *et al.*, 2011; Wase *et al.*, 2014), *Prochlorococcus marinus* (Tolonen *et al.*, 2006), and *Auxenochlorella protothecoides* (Andeden *et al.*, 2021) under N^- condition. We also observed an accumulation of fatty acid in maize roots under N^-. The flux of reactions producing octadecanoic acid, hexadecanoyl-CoA, dodecanoic acid, octanoic acid, and hexadecenoic acid significantly increased under N^-. A similar pattern of accumulation was observed for different unsaturated fatty acids (e.g. icosenoic acid, icosadienoic acid, behenic acid, nervonic acid, arachidic acid, and lignoceric acid). To facilitate growth at the vegetative stage of plant development, plants maintain a certain stoichiometry in C, N, and phosphorus content (Ye *et al.*, 2014). This stoichiometry represents an optimal incorporation of macronutrients in order to produce biomass. However, if there is a shortage of N, C cannot be incorporated into N-containing molecules to sustain root growth and is thus stored as fatty acid when the C:N cellular ratio is higher (Wase *et al.*, 2014). Hence, accumulation of fatty acids in maize roots appears to be an important metabolic signature representative of N deficiency.

Several amino acids act as precursors for the synthesis of important plant secondary metabolites and signaling molecules which play important physiological roles in a number of abiotic stresses. These signaling molecules, such as polyamines, are derived from arginine (Alcázar *et al.*, 2006). Proline is another type of molecule that accumulates, acting as an osmoprotectant or a compatible solute, during abiotic stresses (Per *et al.*, 2017). The family of amino acids derived from aspartate are also involved in energy production under abiotic stress conditions (Kirma *et al.*, 2012). In plants, where hormone levels are modified under various abiotic stresses, cysteine acts as one of the essential precursors (Amir, 2010). Similarly, other amino acids such as lysine play an important role as a precursor for the synthesis of a number of metabolites involved in immune signaling when there is an abiotic stress (Chen *et al.*, 2018; Hartmann *et al.*, 2018), and glycine, serine, and threonine are involved in phospholipid synthesis (Wattenberg, 2021). A broad spectrum of secondary metabolites with multiple biological functions are further derived from the aromatic amino acids, such as phenylalanine, tyrosine, and tryptophan, or from intermediates of their synthesis pathways (Tzin and Galili, 2010). Plants have evolved different strategies to minimize the adverse effects of abiotic stress conditions, and several of them are connected to amino acid metabolism (Hildebrandt, 2018). A general accumulation of amino acids was observed in different plants exposed to abiotic stresses (Lugan *et al.*, 2010; Aleksza *et al.*, 2017; Huang and Jander, 2017; Ferreira Júnior *et al.*, 2018; Batista-Silva *et al.*, 2019). In this study, an accumulation of amino acids was also observed under N^- condition. Overall, under N^-, the flux of all reactions involved in arginine–proline, alanine–aspartate–glutamate, cysteine–methionine, valine–leucine–isoleucine, and histidine biosynthesis showed elevated reaction flux. In the β-alanine pathway, under N^-, most of the reactions showed elevated reaction flux, except for the degradation of 3-oxopropanoate to acetyl-CoA, which exhibited reduced reaction flux. As acetyl-CoA is the precursor of fatty acid biosynthesis, to meet the increasing fatty acid demand, an increased dissociation of malonyl-CoA to acetyl-CoA during β-alanine biosynthesis was observed. In the glycine–serine–threonine biosynthesis pathway, similar to β-alanine, most of the reactions showed elevated fluxes under N^-. Interestingly, under N^- condition, interconversion between glycine and threonine was in favor of threonine production. The experimental metabolomics data also showed that there was an increase in threonine compared with that observed for glycine (Fig. 6). Similarly, in the phenylalanine–tyrosine–tryptophan biosynthesis pathway, most of the reactions showed elevated flux, except for the reactions in the linear pathway, producing chorismite from shikimic acid.

In plants, increased starch accumulation in the leaves is another metabolic reprogramming observed under N^-, such as in duckweed (Yu *et al.*, 2017), Arabidopsis (Krapp *et al.*, 2011), and maize (Amiour *et al.*, 2012). In this study, a similar pattern of starch accumulation in the roots was observed. Reaction flux from amylose to starch showed elevated flux. Similarly, the dissociation of starch to α-D-glucose-1 phosphate showed reduced flux under N^- condition. Starch functions as one of the largest sources of C sink in a plant. During vegetative growth, the roots and immature leaves are the largest C sinks. Then, following the transition to reproductive growth, floral, reproductive, and storage organs become the largest sinks for C. However, if nutrients become limited at any stage of the life cycle, more C is allocated to the roots in order to increase soil mineral acquisition, resulting in a shift in the relative sink balance and C partitioning within the plant (Eghball and Maranville, 1993). In N^- condition, a similar pattern of partitioning was observed for other C sinks such as lignins, where the linear pathway from *p*-coumaric acid to *p*-hydroxy-phenyl lignin showed an increased flux. Overall, this metabolic reprogramming under N^- provided important insights relating to the phenotypic changes of the roots in relation to the underlying metabolism.

In this work, a GSM for maize root was reconstructed which, upon incorporation of omics data, revealed important metabolic reprogramming under N^- condition. The reconstruction of the maize root GSM predicted the increased root biomass production under N^-. Beside predicting important metabolic reprogramming in CCM, fatty acid metabolism, amino acid metabolism, and several other secondary metabolisms, maize root GSM also revealed that several metabolites, such as L-methionine, L-asparagine, L-lysine, cholesterol, and L-pipecolate, were important compounds involved in

root biomass production. Furthermore, this study revealed that eight PC and PF metabolites, not directly coupled with biomass production, played an important role in root growth under N^- condition.

Future research will be focused on the reconstruction of tissue-specific models for kernel, stalk, and tassel. Then, this root GSM will be combined with those tissue-specific models and the previously reconstructed maize leaf model (Simons *et al.*, 2014) to develop a whole-plant maize GSM. A whole-plant GSM will be useful to elucidate the flow of different micro- and macronutrients from the root to the shoots and to the reproductive organs in a maize plant. Furthermore, a whole-plant maize GSM will allow the study of metabolic reprogramming under various other stress conditions such as phosphate deficiency, salinity, drought and thermal stresses, heavy metal accumulation, elevated levels of CO_2, and in the presence of beneficial soil microorganisms. Such studies will allow the identification of key metabolic pathways and markers representative of these stresses, which can potentially be used to select maize genotypes adaptive to diverse favorable or unfavorable environmental conditions.

Supplementary data

The following supplementary data are available at *JXB* online.

Fig. S1. Number of reactions in each category for flux range of different metabolic pathways.

Table. S1. Genome-scale metabolic model of maize root in systems biology markup language.

Table. S2. Experimental transcriptomics data, metabolomics data, and biomass composition.

Table. S3. Arabidopsis validation.

Table. S4. Lipid analysis.

Table. S5. Flux-sum level in each condition.

Acknowledgements

The authors thank Mohammad Mazharul Islam for constructive comments on the manuscript. We also thank Drs Gilles Clément, Gregory Mouille, and Martine Miquel for performing the metabolome and some of the biomass component analyses which were carried out at the Obervatoire du Végétal Chimie Metabolisme of the Institute Jean-Pierre Bourgin, INRA, Versailles-Grignon. The authors declare that they have no conflict of interest.

Author contributions

RS, CDM, and BH: conceptualization; RS: supervision; NA, IQ, and BH: performing the experimental studies and analyses; NBC: performing all *in silico* experiments and analyses; NBC, WLS, and DS: development of the required software programs, models, and graphics; NBC: writing the original manuscript; RS, BH, and CDM: editing. All authors have reviewed and approved the submission of the manuscript.

Funding

We gratefully acknowledge funding support from National Science Foundation (NSF) CAREER grant (25-1106-0039-001), NSF EPSCoR Center for Root and Rhizobiome Innovation grant (25-1215-0139-025) at the University of Nebraska – Lincoln, and The Center for Bioenergy Innovation, a U.S. Department of Energy Research Center supported by the Office of Biological and Environmental Research in the DOE Office of Science.

Data availability

The data that support for the findings of this study can be found in the related cited articles and/or in the supplementary data. All the codes used to generate these results can be directly accessed in the GitHub directory (https://github.com/ssbio/Maize-root-genome-scale-metabolic-model).

References

Alcázar R, Marco F, Cuevas JC, Patron M, Ferrando A, Carrasco P, Tiburcio AF, Altabella T. 2006. Involvement of polyamines in plant response to abiotic stress. Biotechnology Letters **28**, 1867–1876.

Aleksza D, Horváth GV, Sándor G, Szabados L. 2017. Proline accumulation is regulated by transcription factors associated with phosphate starvation. Plant Physiology **175**, 555–567.

Ali U, Li H, Wang X, Guo L. 2018. Emerging roles of sphingolipid signaling in plant response to biotic and abiotic stresses. Molecular Plant **11**, 1328–1343.

Amiour N, Imbaud S, Clément G, *et al.* 2012. The use of metabolomics integrated with transcriptomic and proteomic studies for identifying key steps involved in the control of nitrogen metabolism in crops such as maize. Journal of Experimental Botany **63**, 5017–5033.

Amir R. 2010. Current understanding of the factors regulating methionine content in vegetative tissues of higher plants. Amino Acids **39**, 917–931.

Andeden EE, Ozturk S, Aslim B. 2021. Effect of alkaline pH and nitrogen starvation on the triacylglycerol (TAG) content, growth, biochemical composition, and fatty acid profile of *Auxenochlorella protothecoides* KP7. Journal of Applied Phycology **33**, 211–225.

Arnold A, Nikoloski Z. 2014. Bottom-up metabolic reconstruction of Arabidopsis and its application to determining the metabolic costs of enzyme production. Plant Physiology **165**, 1380–1391.

Bateman A. 2019. UniProt: a worldwide hub of protein knowledge. Nucleic Acids Research **47**, D506–D515.

Batista-Silva W, Heinemann B, Rugen N, Nunes-Nesi A, Araújo WL, Braun HP, Hildebrandt TM. 2019. The role of amino acid metabolism during abiotic stress release. Plant, Cell & Environment **42**, 1630–1644.

Becker SA, Palsson BO. 2008. Context-specific metabolic networks are consistent with experiments. PLoS Computational Biology **4**, e1000082.

Brandes A, Lun DS, Ip K, Zucker J, Colijn C, Weiner B, Galagan JE. 2012. Inferring carbon sources from gene expression profiles using metabolic flux models. PLoS One **7**, e36947.

Cai H, Lu Y, Xie W, Zhu T, Lian X. 2012. Transcriptome response to nitrogen starvation in rice. Journal of Biosciences **37**, 731–747.

Chan SHJ, Cai J, Wang L, Simons-Senftle MN, Maranas CD. 2017. Standardizing biomass reactions and ensuring complete mass balance in genome-scale metabolic models. Bioinformatics **33**, 3603–3609.

Chandrasekaran S, Price ND. 2010. Probabilistic integrative modeling of genome-scale metabolic and regulatory networks in *Escherichia coli* and *Mycobacterium tuberculosis*. Proceedings of the National Academy of Sciences, USA **107**, 17845–17850.

Chatterjee A, Huma B, Shaw R, Kundu S. 2017. Reconstruction of *Oryza sativa indica* genome scale metabolic model and its responses to varying RuBisCO activity, light intensity, and enzymatic cost conditions. Frontiers in Plant Science **8**, 2060.

Chen YC, Holmes EC, Rajniak J, Kim JG, Tang S, Fischer CR, Mudgett MB, Sattely ES. 2018. N-hydroxy-pipecolic acid is a mobile metabolite that induces systemic disease resistance in Arabidopsis. Proceedings of the National Academy of Sciences, USA **115**, E4920–E4929.

Cheung CYM, Williams TCR, Poolman MG, Fell DA, Ratcliffe RG, Sweetlove LJ. 2013. A method for accounting for maintenance costs in flux balance analysis improves the prediction of plant cell metabolic phenotypes under stress conditions. The Plant Journal **75**, 1050–1061.

Chung BK, Lee DY. 2009. Flux-sum analysis: a metabolite-centric approach for understanding the metabolic network. BMC Systems Biology **3**, 117.

Coïc Y, Lesaint C. 1971. Comment assurer une bonne nutrition en eau et en ions minéraux en horticulture. Horticulture Française **8**, 11–14.

Colijn C, Brandes A, Zucker J, Lun DS, Weiner B, Farhat MR, Cheng TY, Moody DB, Murray M, Galagan JE. 2009. Interpreting expression data with metabolic flux models: predicting *Mycobacterium tuberculosis* mycolic acid production. PLoS Computational Biology **5**, e1000489.

Costa-Gutierrez SB, Lami MJ, Santo MCC, Zenoff AM, Vincent PA, Molina-Henares MA, Espinosa-Urgel M, de Cristóbal RE. 2020. Plant growth promotion by *Pseudomonas putida* KT2440 under saline stress: role of eptA. Applied Microbiology and Biotechnology **104**, 4577–4592.

Cotton TEA, Pétriacq P, Cameron DD, Meselmani MA, Schwarzenbacher R, Rolfe SA, Ton J. 2019. Metabolic regulation of the maize rhizobiome by benzoxazinoids. The ISME Journal **13**, 1647–1658.

de Oliveira Dal'Molin CG, Quek LE, Palfreyman RW, Brumbley SM, Nielsen LK. 2010. AraGEM, a genome-scale reconstruction of the primary metabolic network in Arabidopsis. Plant Physiology **152**, 579–589.

Doncheva S, Stoyanova Z, Georgieva K, Nedeva D, Dikova R, Zehirov G, Nikolova A. 2006. Exogenous succinate increases resistance of maize plants to copper stress. Journal of Plant Nutrition and Soil Science **169**, 247–254.

Downs GS, Bi YM, Colasanti J, Wu W, Chen X, Zhu T, Rothstein SJ, Lukens LN. 2013. A developmental transcriptional network for maize defines coexpression modules. Plant Physiology **161**, 1830–1843.

Eghball B, Maranville JW. 1993. Root development and nitrogen influx of corn genotypes under combined drought and nitrogen stresses. Agronomy Journal **85**, 147–152.

Ferreira Júnior DC, Gaion LA, Sousa Júnior GS, Santos DMM, Carvalho RF. 2018. Drought-induced proline synthesis depends on root-to-shoot communication mediated by light perception. Acta Physiologiae Plantarum **40**, 1–5.

Fiehn O. 2006. Metabolite profiling in Arabidopsis. Methods in Molecular Biology **323**, 439–447.

Flores-Tinoco CE, Tschan F, Fuhrer T, Margot C, Sauer U, Christen M, Christen B. 2020. Co-catabolism of arginine and succinate drives symbiotic nitrogen fixation. Molecular Systems Biology **16**, 1–18.

Frey M, Schullehner K, Dick R, Fiesselmann A, Gierl A. 2009. Benzoxazinoid biosynthesis, a model for evolution of secondary metabolic pathways in plants. Phytochemistry **70**, 1645–1651.

Gaude N, Bréhélin C, Tischendorf G, Kessler F, Dörmann P. 2007. Nitrogen deficiency in Arabidopsis affects galactolipid composition and gene expression and results in accumulation of fatty acid phytyl esters. The Plant Journal **49**, 729–739.

Gilbert GA, Gadush MV, Wilson C, Madore MA. 1998. Amino acid accumulation in sink and source tissues of *Coleus blumei* Benth. during salinity stress. Journal of Experimental Botany **49**, 107–114.

Grafahrend-Belau E, Schreiber F, Koschützki D, Junker BH. 2009. Flux balance analysis of barley seeds: a computational approach to study systemic properties of central metabolism. Plant Physiology **149**, 585–598.

Guan JC, Koch KE, Suzuki M, Wu S, Latshaw S, Petruff T, Goulet C, Klee HJ, McCarty DR. 2012. Diverse roles of strigolactone signaling in maize architecture and the uncoupling of a branching-specific subnetwork. Plant Physiology **160**, 1303–1317.

Hartmann M, Zeier T, Bernsdorff F, *et al.* 2018. Flavin monooxygenase-generated N-hydroxypipecolic acid is a critical element of plant systemic immunity. Cell **173**, 456–469.

Hay J, Schwender J. 2011. Computational analysis of storage synthesis in developing *Brassica napus* L. (oilseed rape) embryos: flux variability analysis in relation to ^{13}C metabolic flux analysis. The Plant Journal **67**, 513–525.

Hildebrandt TM. 2018. Synthesis versus degradation: directions of amino acid metabolism during Arabidopsis abiotic stress response. Plant Molecular Biology **98**, 121–135.

Hirel B, Martin A, Tercé-Laforgue T, Gonzalez-Moro MB, Estavillo JM. 2005. Physiology of maize I: a comprehensive and integrated view of nitrogen metabolism in a C4 plant. Physiologia Plantarum **124**, 167–177.

Hockin NL, Mock T, Mulholland F, Kopriva S, Malin G. 2012. The response of diatom central carbon metabolism to nitrogen starvation is different from that of green algae and higher plants. Plant Physiology **158**, 299–312.

Hu B, Chu C. 2020. Nitrogen–phosphorus interplay: old story with molecular tale. New Phytologist **225**, 1455–1460.

Huang T, Jander G. 2017. Abscisic acid-regulated protein degradation causes osmotic stress-induced accumulation of branched-chain amino acids in *Arabidopsis thaliana*. Planta **246**, 737–747.

Huergo LF, Dixon R. 2015. The emergence of 2-oxoglutarate as a master regulator metabolite. Microbiology and Molecular Biology Reviews **79**, 419–435.

Hufford MB, Seetharam AS, Woodhouse MR, *et al.* 2021. De novo assembly, annotation, and comparative analysis of 26 diverse maize genomes. Science **373**, 655–662.

International Grains Council. 2019. Five-year baseline projections of supply and demand for wheat, maize (corn), rice and soyabeans to 2023/24. https://www.igc.int/en/markets/5yeardownload.aspx?mode=download

James GO, Hocart CH, Hillier W, Chen H, Kordbacheh F, Price GD, Djordjevic MA. 2011. Fatty acid profiling of *Chlamydomonas reinhardtii* under nitrogen deprivation. Bioresource Technology **102**, 3343–3351.

Jensen PA, Papin JA. 2011. Functional integration of a metabolic network model and expression data without arbitrary thresholding. Bioinformatics **27**, 541–547.

Kanehisa M, Goto S, Sato Y, Kawashima M, Furumichi M, Tanabe M. 2014. Data, information, knowledge and principle: back to metabolism in KEGG. Nucleic Acids Research **42**, D199–D205.

Kirma M, Araújo WL, Fernie AR, Galili G. 2012. The multifaceted role of aspartate-family amino acids in plant metabolism. Journal of Experimental Botany **63**, 4995–5001.

Krapp A, Berthomé R, Orsel M, Mercey-Boutet S, Yu A, Castaings L, Elftieh S, Major H, Renou JP, Daniel-Vedele F. 2011. Arabidopsis roots and shoots show distinct temporal adaptation patterns toward nitrogen starvation. Plant Physiology **157**, 1255–1282.

Lewis NE, Hixson KK, Conrad TM, *et al.* 2010. Omic data from evolved *E. coli* are consistent with computed optimal growth from genome-scale models. Molecular Systems Biology **6**, 390.

Lugan R, Niogret MF, Leport L, Guégan JP, Larher FR, Savouré A, Kopka J, Bouchereau A. 2010. Metabolome and water homeostasis analysis of *Thellungiella salsuginea* suggests that dehydration tolerance is a key response to osmotic stress in this halophyte. The Plant Journal **64**, 215–229.

Mager S, Ludewig U. 2018. Massive loss of DNA methylation in nitrogen-, but not in phosphorus-deficient *Zea mays* roots is poorly correlated with gene expression differences. Frontiers in Plant Science **9**, 497.

Mahadevan R, Schilling CH. 2003. The effects of alternate optimal solutions in constraint-based genome-scale metabolic models. Metabolic Engineering **5**, 264–276.

Mardanov A, Samedovam A, Shirvany T. 1998. Root–shoot relationships in plant adaptation to nitrogen deficiency. In: Box JE, ed. Root demographics and their efficiencies in sustainable agriculture, grasslands

and forest ecosystems. Developments in Plant and Soil Sciences, vol 82. Dordrecht: Springer, 147–154.

Marisa L, Ichanté JL, Reymond N, Aggerbeck L, Delacroix H, Mucchielli-Giorgi MH. 2007. MAnGO: an interactive R-based tool for two-colour microarray analysis. Bioinformatics **23**, 2339–2341.

Medina MÁ. 2020. Metabolic reprogramming is a hallmark of metabolism itself. BioEssays **42**, 1–10.

Monaco MK, Sen TZ, Dharmawardhana PD, *et al.* 2013. Maize metabolic network construction and transcriptome analysis. The Plant Genome **6**, 1–12.

Naidu BP, Paleg LG, Aspinall D, Jennings AC, Jones GP. 1991. Amino acid and glycine betaine accumulation in cold-stressed wheat seedlings. Phytochemistry **30**, 407–409.

Neal AL, Ahmad S, Gordon-Weeks R, Ton J. 2012. Benzoxazinoids in root exudates of maize attract *Pseudomonas putida* to the rhizosphere. PLoS One **7**, e35498.

Niemeyer HM. 2009. Hydroxamic acids derived from 2-hydroxy-2H-1,4-benzoxazin-3(4H)-one: key defense chemicals of cereals. Journal of Agricultural and Food Chemistry **57**, 1677–1696.

Oddy J, Raffan S, Wilkinson MD, Elmore JS, Halford NG. 2020. Stress, nutrients and genotype—understanding and managing asparagine accumulation in wheat grain. CABI Agriculture and Bioscience **1**, 10.

Oldroyd GED, Leyser O. 2020. A plant's diet, surviving in a variable nutrient environment. Science **368**, eaba0196.

Orth JD, Thiele I, Palsson BØ. 2010. What is flux balance analysis? Nature Biotechnology **28**, 245–248.

Per TS, Khan NA, Reddy PS, Masood A, Hasanuzzaman M, Khan MIR, Anjum NA. 2017. Approaches in modulating proline metabolism in plants for salt and drought stress tolerance: phytohormones, mineral nutrients and transgenics. Plant Physiology and Biochemistry **115**, 126–140.

Pilalis E, Chatziioannou A, Thomasset B, Kolisis F. 2011. An in silico compartmentalized metabolic model of *Brassica napus* enables the systemic study of regulatory aspects of plant central metabolism. Biotechnology and Bioengineering **108**, 1673–1682.

Poolman MG, Kundu S, Shaw R, Fell DA. 2013. Responses to light intensity in a genome-scale model of rice metabolism. Plant Physiology **162**, 1060–1072.

Poolman MG, Miguet L, Sweetlove LJ, Fell DA. 2009. A genome-scale metabolic model of Arabidopsis and some of its properties. Plant Physiology **151**, 1570–1581.

Puig J, Pauluzzi G, Guiderdoni E, Gantet P. 2012. Regulation of shoot and root development through mutual signaling. Molecular Plant **5**, 974–983.

Roberts JK, Lane AN, Clark RA, Nieman RH. 1985. Relationships between the rate of synthesis of ATP and the concentrations of reactants and products of ATP hydrolysis in maize root tips, determined by ^{31}P nuclear magnetic resonance. Archives of Biochemistry and Biophysics **240**, 712–722.

Rouf Shah T, Prasad K, Kumar P. 2016. Maize—a potential source of human nutrition and health: a review. Cogent Food & Agriculture **2**, https://doi.org/10.1080/23311932.2016.1166995

Saha R, Suthers PF, Maranas CD. 2011. *Zea mays* iRS1563: a comprehensive genome-scale metabolic reconstruction of maize metabolism. PLoS One **6**, e21784.

Satish Kumar V, Dasika MS, Maranas CD. 2007. Optimization based automated curation of metabolic reconstructions. BMC Bioinformatics **8**, 212.

Schlüter U, Mascher M, Colmsee C, Scholz U, Bräutigam A, Fahnenstich H, Sonnewald U. 2012. Maize source leaf adaptation to nitrogen deficiency affects not only nitrogen and carbon metabolism but also control of phosphate homeostasis. Plant Physiology **160**, 1384–1406.

Seaver SMD, Bradbury LMT, Frelin O, Zarecki R, Ruppin E, Hanson AD, Henry CS. 2015. Improved evidence-based genome-scale metabolic models for maize leaf, embryo, and endosperm. Frontiers in Plant Science **6**, 142.

Shaw R, Cheung CYM. 2019. A mass and charge balanced metabolic model of *Setaria viridis* revealed mechanisms of proton balancing in C4 plants. BMC Bioinformatics **20**, 357.

Shaw R, Cheung CYM. 2020. Multi-tissue to whole plant metabolic modelling. Cellular and Molecular Life Sciences **77**, 489–495.

Simons M, Saha R, Amiour N, *et al.* 2014. Assessing the metabolic impact of nitrogen availability using a compartmentalized maize leaf genome-scale model. Plant Physiology **166**, 1659–1674.

Spiegel S, Milstien S. 2003. Sphingosine-1-phosphate: an enigmatic signalling lipid. Nature Reviews. Molecular Cell Biology **4**, 397–407.

Sun H, Tao J, Gu P, Xu G, Zhang Y. 2016. The role of strigolactones in root development. Plant Signaling & Behavior **11**, e1110662.

Tercé-Laforgue T, Mäck G, Hirel B. 2004. New insights towards the function of glutamate dehydrogenase revealed during source–sink transition of tobacco (*Nicotiana tabacum*) plants grown under different nitrogen regimes. Physiologia Plantarum **120**, 220–228.

Tolonen AC, Aach J, Lindell D, Johnson ZI, Rector T, Steen R, Church GM, Chisholm SW. 2006. Global gene expression of Prochlorococcus ecotypes in response to changes in nitrogen availability. Molecular Systems Biology **2**, 53.

Tschoep H, Gibon Y, Carillo P, Armengaud P, Szecowka M, Nunes-Nesi A, Fernie AR, Koehl K, Stitt M. 2009. Adjustment of growth and central metabolism to a mild but sustained nitrogen-limitation in Arabidopsis. Plant, Cell & Environment **32**, 300–318.

Tzin V, Galili G. 2010. New insights into the shikimate and aromatic amino acids biosynthesis pathways in plants. Molecular Plant **3**, 956–972.

Vriet C, Russinova E, Reuzeau C. 2012. Boosting crop yields with plant steroids. The Plant Cell **24**, 842–857.

Walton A, Stes E, Goeminne G, *et al.* 2016. The response of the root proteome to the synthetic strigolactone GR24 in Arabidopsis. Molecular & Cellular Proteomics **15**, 2744–2755.

Wase N, Black PN, Stanley BA, DiRusso CC. 2014. Integrated quantitative analysis of nitrogen stress response in *Chlamydomonas reinhardtii* using metabolite and protein profiling. Journal of Proteome Research **13**, 1373–1396.

Wattenberg BW. 2021. Kicking off sphingolipid biosynthesis: structures of the serine palmitoyltransferase complex. Nature Structural & Molecular Biology **28**, 229–231.

Yamaya T, Matsumoto H. 1989. Accumulation of asparagine in NaCl-stressed barley seedlings. Berichte der Ohara Instituts für landwirtschaftliche **19**, 181–188.

Ye Y, Liang X, Chen Y, Li L, Ji Y, Zhu C. 2014. Carbon, nitrogen and phosphorus accumulation and partitioning, and C:N:P stoichiometry in late-season rice under different water and nitrogen managements. PLoS One **9**, e101776.

Yesbergenova-Cuny Z, Dinant S, Martin-Magniette ML, Quilleré I, Armengaud P, Monfalet P, Lea PJ, Hirel B. 2016. Genetic variability of the phloem sap metabolite content of maize (*Zea mays* L.) during the kernel-filling period. Plant Science **252**, 347–357.

Yu C, Zhao X, Qi G, Bai Z, Wang Y, Wang S, Ma Y, Liu Q, Hu R, Zhou G. 2017. Integrated analysis of transcriptome and metabolites reveals an essential role of metabolic flux in starch accumulation under nitrogen starvation in duckweed. Biotechnology for Biofuels **10**, 167.

Zur H, Ruppin E, Shlomi T. 2010. iMAT: an integrative metabolic analysis tool. Bioinformatics **26**, 3140–3142.